Available online at www.sciencedirect.com

ScienceDirect

Procedia Structural Integrity 39 (2022) 148–156

Structural Integrity Procedia

www.elsevier.com/locate/procedia

7th International Conference on Crack Paths

Stress-intensity factor solutions for the simulation of fish-eye fatigue crack growth in round bars subjected to tensile load

J.M Alegre[a]*, I.I. Cuesta[a], A. Díaz[a]

[a]*University of Burgos. Escuela Politécnica Superior, Av de Cantabria s/n, Burgos, 09006, Spain*

Abstract

The fatigue crack growth in round bars initiated from internal defects leads to the formation of a circular crack pattern usually so-called *fish-eye*. This failure mechanism is found in the current additive manufacturing techniques in which internal defects, such as pores or lack of fusion, are the main cause of fatigue crack initiation. Moreover, this fatigue mechanism becomes the predominant failure mode in the Very High Cycle Fatigue (VHCF) regime. With the aim of adequately studying these fatigue crack situations, this paper presents a set of solutions for the stress-intensity factor calculation for embedded elliptical cracks in a round bar subjected to tensile load. The stress-intensity factors (SIF) are presented in a tabulated form and were obtained from three-dimensional finite-element analyses. The SIF solutions are provided as a function of three dimensionless parameters that include the crack size, the crack aspect ratio, and its relative position in the cross section. After that, a sequential methodology for fatigue crack growth simulation is presented, and a comparison with experimental results of fatigue crack propagation initiated from internal defects in round bars is also presented. Finally, by varying the initial crack position and the initial crack aspect ratio, several aspects related to the evolution of the fatigue crack shape in this geometry are analyzed.

Keywords: Embedded cracks; fish-eye; round bars

* Corresponding author. Tel.: +34 947258920.
E-mail address: jalegre@ubu.es

10.1016/j.prostr.2022.03.083

1. Introduction

Additive Manufacturing (AM) techniques are increasingly being used for high critical components in aerospace, biomedical and automotive sectors. However, the main problem of AM is presence of internal defects, lack of fusion or pores, which are the main cause of fatigue crack initiation in these components (Benedetti et al., 2018; Hu et al., 2020). These internal defects grow due to fatigue until failure occurs, forming a circular crack pattern on the fracture surface, the so-called *fish-eye* (Figure 1). This fatigue mechanism also becomes the predominant failure mode in the Very High Cycle Fatigue (VHCF) regime (Günther et al., 2017).

Some numerical studies of the *fish-eye* crack growth can be found in the literature (Marines-Garcia et al., 2008; Nguyen et al., 2015; Sun et al., 2016). However, the crack shape is assumed to be circular during the crack growth or, in a more complex analysis, the exact crack growth shape is estimated from a large number of SIFs along the crack front (Nguyen et al., 2015). The purpose of this work is firstly to obtain the SIF solutions for the vertices of elliptical embedded cracks in this geometry, and then to use these calculated SIFs to simulate the *fish-eye* assuming that an elliptical shape is maintained during all the propagation phase. In this way, by varying the initial crack position and the initial crack aspect ratio, several aspects related to the evolution of the fatigue crack shape in this geometry can be analyzed.

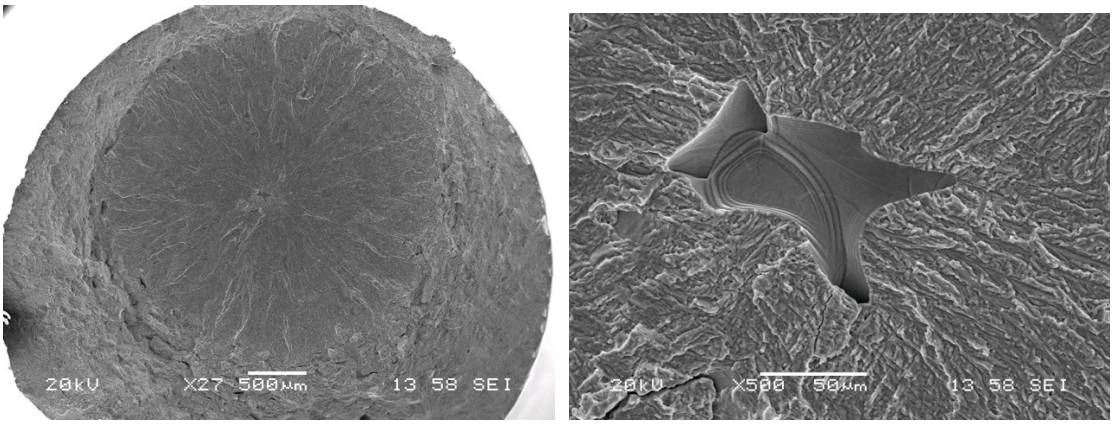

Fig. 1 Fish-eye example in a round bar initiated by fatigue from an internal defect. Material: Ti6Al4V fabricated by SLM.

2. Stress-intensity factor solutions for an embedded crack in a round bar subjected to tensile load

2.1. Geometry definition and dimensionless parameters

The geometry of the round bar and the main dimensions of a generic embedded elliptical crack are presented in Figure 2. The elliptical crack shape and its position in the round bar are defined by three parameters: the semi-axes of the ellipse (a and c) and the position of the center of the crack ($a+h$). The radius of the bar is R, and the tensile applied stress is (σ_0). These geometric dimensions can be expressed by three new dimensionless parameters: $(a+h)/R$ that defines the relative position of the center of the elliptical crack to the radius of the circular cross section; $a/(a+h)$ that defines the ratio of the crack size to the distance from the center of the ellipse to the bar surface; and a/c that defines the aspect ratio of the elliptical crack.

2.2. Finite element model and SIF solutions

In order to obtain the stress-intensity factors for this geometry, a specific 3D finite element model, using Abaqus software, has been created. Only one-fourth of the round bar is modelled because of its symmetry. The mesh was created using 20-node quadratic elements with reduced integration (C3D20R), and a typical spider-web mesh around

the crack tip, using quarter-point finite elements, was used. A mesh density of 8 elements for the semi-rosette of the crack tip was chosen, and the crack front was constructed with 100 elements.

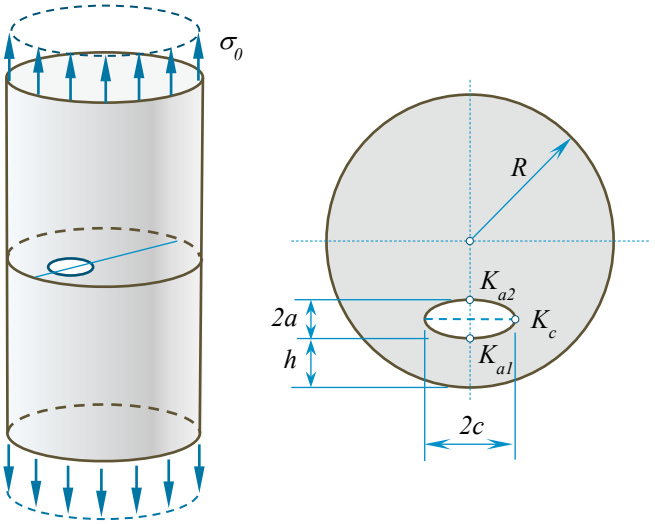

Fig. 2 Geometry definition of the embedded elliptical crack in a round bar.

The SIF values were obtained from the calculation of the *J*-integral parameter. For a linear elastic analysis, the stress-intensity factor value, K_I, is calculated from the elastic part of *J*-integral, J_e, using the following relationship,

$$K_I = \sqrt{J_e \cdot E'} \tag{1}$$

where $E' = E$ for plane stress and $E' = E/(1-\nu^2)$ for plane strain conditions, with E being Young's modulus and ν Poisson's ratio. For an embedded crack, plane strain conditions are assumed for all points along the crack front.

Only the SIF at the vertices of the elliptical crack were calculated (see Figure 2), and are expressed as:

$$K_{a1} = F_{a1} \cdot \sigma_0 \cdot \sqrt{\pi a} \quad ; \quad K_{a2} = F_{a2} \cdot \sigma_0 \cdot \sqrt{\pi a} \quad ; \quad K_c = F_c \cdot \sigma_0 \cdot \sqrt{\pi a} \tag{2}$$

where σ_0 is the uniform axial stress, a is the crack depth, and F_{a1}, F_{a2} and F_c are the geometry correction factors, calculated as a function of the three dimensionless parameters: $a/(a+h)$ ranging from 0.05 to 0.95, $(a+h)/R$ ranging from 1 (centered cracks) to 0.05 (cracks close to the bar surface) and a/c ranging from 0.2 (elongated cracks) to 1.0 (circular cracks). The values of the geometry correction factors obtained are collected on Tables 1 to 3 of Appendix A. A comparison and validation of the proposed SIF solutions with other proven solutions available in the literature can be found in previous works of the authors (Alegre et al., 2021).

3. Fatigue crack growth methodology

For the simulation of the fatigue crack growth a sequential methodology is used. During the fatigue process, the crack is continuously updated assuming an elliptical growth and taking for the calculation the value of the stress intensity factor at the vertices of the semi-axis of the elliptical crack.

The process starts by assuming an initial crack size (*a* and *c*) and its initial position in the cross section defined by the ligament (*h*). The three dimensionless parameters are calculated (a/c, $(a+h)/R$ and $a/(a+h)$) allowing the geometry correction factors to be obtained using Tables 1 to 3. An interpolation procedure is necessary at this stage.

For a fatigue load defined by the stress range $\Delta\sigma$, the stress-intensity factor ranges at the vertices of the elliptical crack are obtained as:

$$\Delta K_{a1} = F_{a1} \cdot \Delta\sigma \cdot \sqrt{\pi a} \quad ; \quad \Delta K_{a2} = F_{a2} \cdot \Delta\sigma \cdot \sqrt{\pi a} \quad ; \quad \Delta K_c = F_c \cdot \Delta\sigma \cdot \sqrt{\pi a} \tag{3}$$

Using these SIF values, and assuming a Paris type fatigue crack growth, $da/dN = C \cdot (\Delta K)^m$, the crack advance of the vertices of the ellipse can be obtained after a defined block of cycles as:

$$\Delta a_1 = \Delta N \cdot C \cdot \left(\Delta K_{a1}\right)^m \quad ; \quad \Delta a_2 = \Delta N \cdot C \cdot \left(\Delta K_{a2}\right)^m \quad ; \quad \Delta c = \Delta N \cdot C \cdot \left(\Delta K_c\right)^m \tag{4}$$

where C and m are the Paris law coefficients, ΔN is the desired number of cycles per block (e.g., $\Delta N = 1000$ cycles) defined by the user. Finally, the new crack size and crack position are updated by means of:

$$\begin{aligned} 2a_{new} &= 2a + \left(\Delta a_1 + \Delta a_2\right) \\ 2c_{new} &= 2c + 2\Delta c \\ h_{new} &= h - \Delta a_1 \end{aligned} \tag{5}$$

The whole procedure is repeated, updating the crack shape for each block of cycles, until the failure condition is reached, or the desired number of cycles is completed. An example of the application of the sequential methodology, using the present SIF solutions, is presented Figure 3.

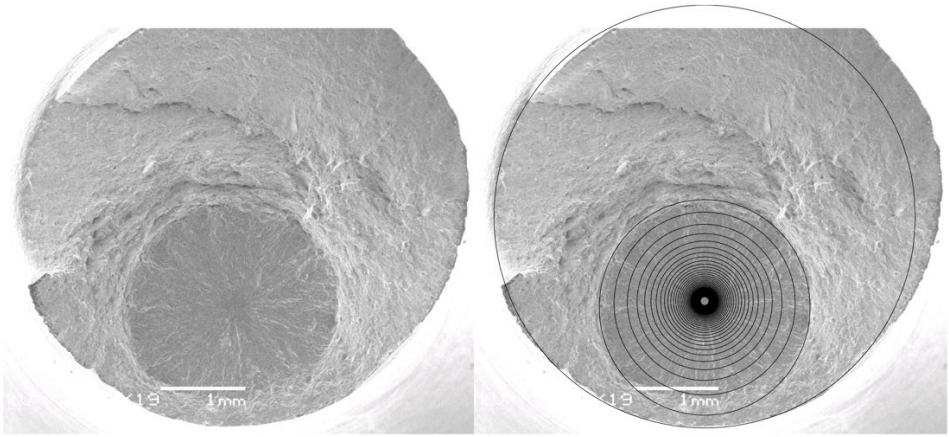

Fig. 3 Experimental and predicted *fish-eye* fatigue crack growth initiated from an internal defect on a round bar subjected to uniaxial tensile load.

4. Prediction of the fatigue crack shape

An interesting fact observed for this geometry is the preferential trend of the crack to propagate toward a circular shape pattern, known as *fish-eye*, independently of the aspect ratio of the initial defect. This fact is also observed experimentally, as presented in Figure 4, where the irregular initial crack shape quickly develops to a circular crack.

The analysis presented in this paragraph corresponds to a specimen of radius $R = 3\,mm$, subjected to a uniaxial stress load of $\sigma_0 = 200\,MPa$, and with an initial flaw in the position $(a_0 + h_0) = 2R/3 = 2\ mm$. The fatigue crack growth law is defined using a Paris equation with material parameters, $C = 2.99 \cdot 10^{-8}$ and $m = 3$ (units in *mm/cycle* and $MPa \cdot m^{1/2}$), typical for a Ti6Al4V alloy fabricated by Selective Laser Melting (Jiao et al., 2017).

Figure 5 shows this preferred trend for various initial elliptical cracks with different aspect ratios, from a circular shape ($a_0 / c_0 = 1$) to a very elongated shape ($a_0 / c_0 = 0.2$) and assuming an initial crack size of $a_0 = 0.05\,mm$. A quick trend to a circular crack shape is observed, regardless of the shape of the initial crack. This trend is faster the smaller the initial flaw and the more centered on the specimen.

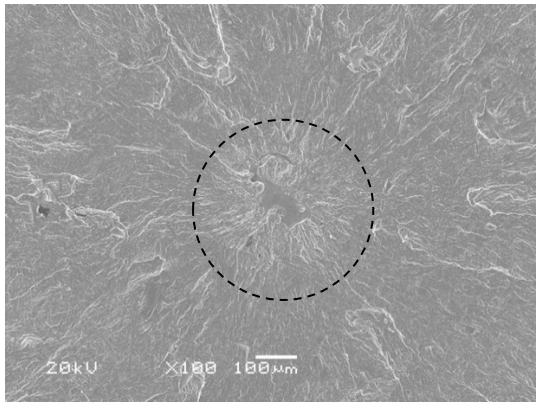

Fig. 4 Propagation towards a circular crack from an initial irregular crack shape. Ti6Al4V fabricated by SLM.

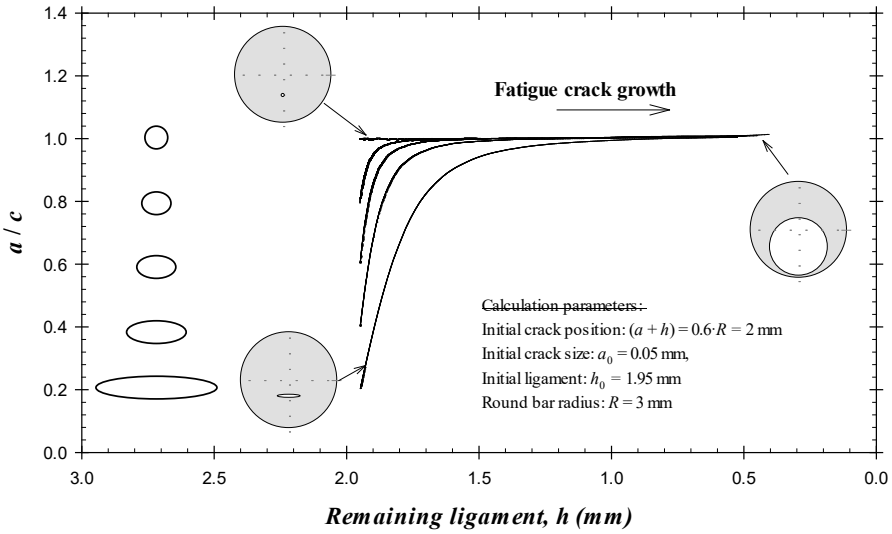

Fig. 5 Simulation of the *fish-eye* crack growth for different initial crack aspect ratios.

The effect of the initial crack shape on the fatigue life is analyzed in Figure 6. The reference value is an initial circular crack of dimensions $a_0 = 0.1mm$, $c_0 = 0.1mm$, with a crack area of $A_0 = \pi a_0 c_0 = 0.031416\ mm^2$. The initial position of the crack is maintained constant as $a_0 + h_0 = 2mm$.

Three curves are presented in this Figure 6. The first curve represents the obtained fatigue life vs. the initial crack aspect ratio, maintaining constant the crack dimension $a_0 = 0.1\ mm$. The second curve is similar, but in this case the crack dimension $c_0 = 0.1mm$ is fixed. And finally, in the third curve the initial crack area $A_0 = \pi a_0 c_0 = 0.031416\ mm^2$ is kept constant for the different crack aspect ratios. The results show that the same fatigue life is obtained when considering different initial crack shapes but maintaining constant the initial crack area. As a result, an equivalent initial crack size (e.g., with a circular shape) can be defined for any irregular initial defect with the same projected area. The *equivalent circular initial crack* size can be then obtained as:

$$a_{0eq} = \sqrt{\frac{area}{\pi}} = 0.5642 \cdot \sqrt{area} \tag{6}$$

where *area* represents the initial projected area of the irregular defect.

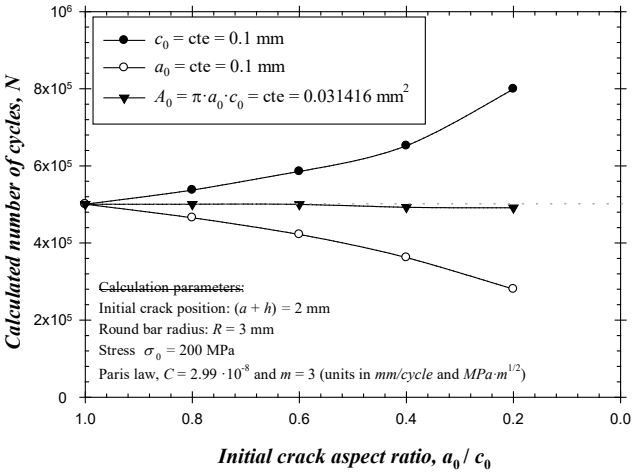

a_0	c_0	a_0 / c_0	A_0	N_{cycles}
0.1	0.1	1	0.031416	486344
0.08	0.1	0.8	0.025133	522063
0.06	0.1	0.6	0.018850	569879
0.04	0.1	0.4	0.012566	635177
0.02	0.1	0.2	0.006283	775922
0.1	0.1	1	0.031416	486344
0.1	0.125	0.8	0.03927	452348
0.1	0.167	0.6	0.05236	409425
0.1	0.25	0.4	0.07854	351189
0.1	0.5	0.2	0.15708	269503
0.1	0.1	1	0.031416	486344
0.0894	0.112	0.8	0.031416	486316
0.0774	0.129	0.6	0.031416	485174
0.0632	0.158	0.4	0.031416	478798
0.0447	0.223	0.2	0.031416	475020

Fig 6. Effect of initial crack shape in the predicted fatigue life of the *fish-eye* crack growth simulation.

These results agree with the model of Murakami (Murakami & Beretta, 1999), which postulates that the maximum stress intensity factor along the crack front of an embedded elliptical crack has a strong correlation with the square root of the initial defect projected crack area, $\sqrt{area}$. They propose this parameter for use as the characteristic dimension for the evaluation of the effects of defects of various sizes and shapes on fatigue strength.

5. Conclusions

1. A good estimation of *fish-eye* crack growth can be carried out by using the proposed SIF solutions for elliptical cracks in a round bar subjected to tensile load.

2. The simulated crack during the *fish-eye* crack growth quickly tends to a very close circular form, regardless of the shape of the initial crack. This effect can be also observed by experiment.

3. The same fatigue life is obtained when considering different initial crack shapes but maintaining constant the initial crack area. These results are in accordance with the model of Murakami, which proposes the square root of the projected crack area, $\sqrt{area}$, as the characteristic dimension for the evaluation of the effects of defects of various sizes and shapes on fatigue strength. As a result, for a fatigue analysis, an equivalent initial crack size (e.g., circular) can be defined for any irregular initial defect, considering the same projected area.

Acknowledgements

The authors gratefully acknowledge financial support from the Junta de Castilla y Leon (Spain) through grant BU-002-P20, co-financed by FEDER funds.

References

Alegre, J. M., Cuesta, I. I., & Díaz, A. (2021). Soluciones del factor de intensidad de tensiones para fisuras elípticas internas en barras cilíndricas sometidas a esfuerzos de tracción. *Revista Española de Mecánica de Fractura*, *2*, 73–79. https://gef.es/images/revista/revista-española-mecanica-fractura-vol2-julio2021.pdf

Benedetti, M., Fontanari, V., Bandini, M., Zanini, F., & Carmignato, S. (2018). Low- and high-cycle fatigue resistance of Ti-6Al-4V ELI additively manufactured via selective laser melting: Mean stress and defect sensitivity. *International Journal of Fatigue*, *107*(October 2017), 96–109. https://doi.org/10.1016/j.ijfatigue.2017.10.021

Günther, J., Krewerth, D., Lippmann, T., Leuders, S., Tröster, T., Weidner, A., Biermann, H., & Niendorf, T. (2017). Fatigue life of additively manufactured Ti–6Al–4V in the very high cycle fatigue regime. *International Journal of Fatigue*, *94*, 236–245. https://doi.org/10.1016/j.ijfatigue.2016.05.018

Hu, Y. N., Wu, S. C., Withers, P. J., Zhang, J., Bao, H. Y. X., Fu, Y. N., & Kang, G. Z. (2020). The effect of manufacturing defects on the fatigue life of selective laser melted Ti-6Al-4V structures. *Materials and Design*, *192*. https://doi.org/10.1016/j.matdes.2020.108708

Jiao, Z. H., Xu, R. D., Yu, H. C., & Wu, X. R. (2017). Evaluation on Tensile and Fatigue Crack Growth Performances of Ti6Al4V Alloy Produced

by Selective Laser Melting. *Procedia Structural Integrity*, *7*, 124–132. https://doi.org/10.1016/j.prostr.2017.11.069

Marines-Garcia, I., Paris, P. C., Tada, H., Bathias, C., & Lados, D. (2008). Fatigue crack growth from small to large cracks on very high cycle fatigue with fish-eye failures. *Engineering Fracture Mechanics*, *75*(6), 1657–1665. https://doi.org/10.1016/j.engfracmech.2007.05.015

Murakami, Y., & Beretta, S. (1999). Small Defects and Inhomogeneities in Fatigue Strength: Experiments , Models and Statistical Implications. *Extremes*, *2*(2), 123–147. https://link.springer.com/content/pdf/10.1023/A:1009976418553.pdf

Nguyen, H. Q., Gallimard, L., & Bathias, C. (2015). Numerical simulation of fish-eye fatigue crack growth in very high cycle fatigue. *Engineering Fracture Mechanics*, *135*, 81–93. https://doi.org/10.1016/j.engfracmech.2015.01.010

Sun, Z., Li, W., Deng, H., & Zhang, Z. (2016). Fisheye failure analysis and life design approach for case-carburized gear steel based on statistical evaluation of defect size. *Engineering Failure Analysis*, *59*, 28–40. https://doi.org/10.1016/j.engfailanal.2015.11.017

Appendix A. Geometry correction factors for an embedded elliptical crack in a round bar

This appendix collects the geometry correction factors (F_{a1}, F_{a2} and F_c) necessary to obtain the stress intensity factor for an embedded elliptical crack in a round bar subjected to tensile load. These geometry correction factors are calculated as a function of the three dimensionless parameters: $a/(a+h)$, $(a+h)/R$, and a/c.

Table 1. Geometry Correction Factor, F_{a1}.

a/c	$\frac{a}{(a+h)}$	$(a+h)/R$ 0.05	0.2	0.4	0.6	0.8	1.0
0.2	**0.05**	0.9481	0.9481	0.9481	0.9481	0.9481	0.9481
	0.2	0.9531	0.9543	0.9582	0.9636	0.9695	-
	0.4	0.9834	0.9967	-	-	-	-
	0.6	1.0649	-	-	-	-	-
	0.8	1.2756	-	-	-	-	-
	0.95	1.9484	-	-	-	-	-
0.4	**0.05**	0.8665	0.8665	0.8665	0.8665	0.8665	0.8665
	0.2	0.8689	0.8694	0.8704	0.8722	0.8744	0.8784
	0.4	0.8871	0.8918	0.9068	0.9285	0.9521	-
	0.6	0.9422	0.9635	1.0347	-	-	-
	0.8	1.0790	1.1586	-	-	-	-
	0.95	1.5754	-	-	-	-	-
0.6	**0.05**	0.7812	0.7812	0.7812	0.7812	0.7812	0.7812
	0.2	0.7823	0.7825	0.7828	0.7835	0.7844	0.7862
	0.4	0.7942	0.7966	0.8029	0.8136	0.8250	0.841
	0.6	0.8317	0.8421	0.8753	0.9262	0.9822	-
	0.8	0.9405	0.9765	1.1007	1.3091	-	-
	0.95	1.2667	1.3855	1.8561	-	-	-
0.8	**0.05**	0.7058	0.7058	0.7058	0.7058	0.7058	0.7058
	0.2	0.7067	0.7068	0.7069	0.7072	0.7076	0.7082
	0.4	0.7146	0.7159	0.7191	0.7246	0.731	0.7396
	0.6	0.7413	0.7474	0.7645	0.7927	0.8216	0.8532
	0.8	0.8216	0.8419	0.9063	1.0135	1.1406	-
	0.95	1.0669	1.1293	1.3360	1.7603	-	-
1	**0.05**	0.6386	0.6386	0.6386	0.6386	0.6386	0.6386
	0.2	0.6388	0.6388	0.6389	0.6391	0.6394	0.6398
	0.4	0.6437	0.6446	0.6463	0.6492	0.6529	0.6582
	0.6	0.6631	0.6671	0.6769	0.6936	0.7108	0.7274
	0.8	0.7239	0.7368	0.7731	0.8347	0.8998	0.9525
	0.95	0.9143	0.9520	1.0637	1.2671	1.5391	1.8441

Table 2. Geometry Correction Factor, F_{a2}.

a/c	$\frac{a}{(a+h)}$	$(a+h)/R$ 0.05	0.2	0.4	0.6	0.8	1.0
0.2	**0.05**	0.9481	0.9481	0.9481	0.9481	0.9481	0.9481
	0.2	0.9521	0.9531	0.9564	0.9608	0.9663	-
	0.4	0.9692	0.9796	-	-	-	-
	0.6	1.0025	-	-	-	-	-
	0.8	1.0436	-	-	-	-	-
	0.95	1.0870	-	-	-	-	-
0.4	**0.05**	0.8663	0.8663	0.8663	0.8663	0.8663	0.8664
	0.2	0.8679	0.8683	0.8692	0.8705	0.8726	0.8781
	0.4	0.8775	0.8808	0.8917	0.9058	0.9256	-
	0.6	0.8951	0.9101	0.9539	-	-	-
	0.8	0.9214	0.9615	-	-	-	-
	0.95	0.9662	-	-	-	-	-
0.6	**0.05**	0.7804	0.7804	0.7804	0.7804	0.7804	0.7804
	0.2	0.7815	0.7813	0.7816	0.7823	0.7839	0.7866
	0.4	0.7882	0.7897	0.7941	0.7995	0.8102	0.8414
	0.6	0.8001	0.8059	0.8241	0.8499	0.8890	-
	0.8	0.8191	0.8354	0.8915	0.9675	-	-
	0.95	0.8357	0.8698	1.0040	-	-	-
0.8	**0.05**	0.7067	0.7067	0.7067	0.7067	0.7067	0.7067
	0.2	0.7071	0.7071	0.7072	0.7074	0.7078	0.7087
	0.4	0.7104	0.7112	0.7131	0.7163	0.7217	0.7402
	0.6	0.7182	0.7213	0.7306	0.7421	0.7637	0.8538
	0.8	0.7304	0.7385	0.7657	0.8001	0.8611	-
	0.95	0.7409	0.7568	0.8129	0.8929	-	-
1	**0.05**	0.6387	0.6386	0.6386	0.6386	0.6386	0.6386
	0.2	0.6392	0.6392	0.6393	0.6395	0.6398	0.6398
	0.4	0.6409	0.6413	0.6422	0.6439	0.6467	0.6582
	0.6	0.6462	0.6479	0.6527	0.6598	0.6719	0.7274
	0.8	0.6543	0.6589	0.6732	0.6913	0.7237	0.9525
	0.95	0.6584	0.6669	0.6959	0.7296	0.7912	1.8441

Table 3. Geometry Correction Factor, F_c.

a/c	$\frac{a}{(a+h)}$	$(a+h)/R$ 0.05	0.2	0.4	0.6	0.8	1.0
0.2	**0.05**	0.4221	0.4221	0.4221	0.4221	0.4221	0.4221
	0.2	0.4236	0.4242	0.4260	0.4291	0.4353	-
	0.4	0.4284	0.4363	-	-	-	-
	0.6	0.4377	-	-	-	-	-
	0.8	0.4545	-	-	-	-	-
	0.95	0.4720	-	-	-	-	-
0.4	**0.05**	0.5477	0.5476	0.5478	0.5478	0.5478	0.5479
	0.2	0.5489	0.5492	0.5499	0.5510	0.5525	0.5559
	0.4	0.5550	0.5578	0.5669	0.5816	0.6100	-
	0.6	0.5666	0.5789	0.6281	-	-	-
	0.8	0.5833	0.6221	-	-	-	-
	0.95	0.6009	-	-	-	-	-
0.6	**0.05**	0.6057	0.6055	0.6057	0.6057	0.6058	0.6058
	0.2	0.6064	0.6065	0.6068	0.6072	0.6079	0.6098
	0.4	0.6120	0.6135	0.6179	0.6252	0.6349	0.6582
	0.6	0.6235	0.6299	0.6514	0.6870	0.7529	-
	0.8	0.6429	0.6624	0.7376	0.9221	-	-
	0.95	0.6567	0.7067	0.9238	-	-	-
0.8	**0.05**	0.6314	0.6314	0.6315	0.6315	0.6315	0.6315
	0.2	0.6318	0.6319	0.6320	0.6322	0.6325	0.6333
	0.4	0.6360	0.6370	0.6393	0.6434	0.6492	0.6623
	0.6	0.6464	0.6504	0.6623	0.6820	0.7090	0.7793
	0.8	0.6642	0.6756	0.7153	0.7835	0.9081	-
	0.95	0.6798	0.7099	0.8018	1.0052	-	-
1	**0.05**	0.6386	0.6386	0.6386	0.6386	0.6386	0.6386
	0.2	0.6389	0.6389	0.6390	0.6392	0.6395	0.6398
	0.4	0.6417	0.6423	0.6436	0.6459	0.6495	0.6582
	0.6	0.6504	0.6531	0.6602	0.6725	0.6889	0.7274
	0.8	0.6660	0.6736	0.6972	0.7367	0.7926	0.9525
	0.95	0.6861	0.6965	0.7487	0.8423	1.0031	1.8441